PHYSICS OF FLUIDS **25**, 046601 (2013)

Geostrophic turbulence near rapid changes in stratification

K. S. Smith[1,a)] and E. Bernard[2]
[1]*Center for Atmosphere Ocean Science, Courant Institute of Mathematical Sciences, New York University, New York, New York 10012, USA*
[2]*Institut Curie, 26 Rue d'Ulm, 75005 Paris, France*

(Received 2 January 2013; accepted 19 March 2013; published online 11 April 2013)

Geostrophic turbulence near horizontal surfaces on which the vertical velocity vanishes exhibits a forward cascade of buoyancy variance, characterized by a shallow energy spectrum, secondary roll-up of filaments, and a fat-tailed vorticity probability distribution. Such surfaces occur at rigid boundaries, but also at discontinuous jumps in stratification. Here we relax this mathematical idealization and investigate geostrophic turbulence near a rapid but smooth jump in stratification, modeled by $N(z) = N_0[1 + \alpha \tanh(z/h)]$. The rapidity of change is controlled by the length scale h and the profile approaches a step function as $h \to 0$. The approximated Green's function for the quasigeostrophic potential vorticity (PV) is used to predict the spectral PV-streamfunction relationship, under various assumptions about the distribution of the initial PV. Numerical simulations of freely-evolving quasigeostrophic turbulence in the presence of the model stratification support the predictions and reveal that the jump has two effects: it alters the Green's function in the region of the jump and it produces a peak in PV near the jump, approaching a Dirac delta-function as the jump scale $h \to 0$. When the Green's function is integrated against this sharp PV distribution, contributions far from the jump ($|z| \gg h$) are suppressed and the flow in a region $|z| \lesssim O(h)$ exhibits surface effects. This occurs for horizontal scales $L \gtrsim N_0 h/f$, the deformation scale associated with the jump. These results have implications for geostrophic turbulence near the tropopause in the atmosphere and the base of the mixed layer in the ocean. © *2013 American Institute of Physics*. [http://dx.doi.org/10.1063/1.4799470]

I. INTRODUCTION

Charney's theory of geostrophic turbulence[1] predicts that a quasigeostrophic system forced by narrow-band stirring will exhibit an inverse cascade of total energy above the forcing scale and a forward cascade of potential enstrophy below it, with a wavenumber energy spectrum with spectral slopes of $-5/3$ and -3, respectively. The theory is based on the close analogy between the two-dimensional vorticity equation and the quasigeostrophic (QG) equations, which are

$$\partial_t q + J(\psi, q) = 0, \quad \text{where} \quad q = \nabla^2 \psi + \partial_z \left(\frac{f^2}{N^2} \partial_z \psi \right) \tag{1}$$

is the QG potential vorticity (PV), f is the Coriolis parameter, $N(z)$ is the buoyancy frequency, $\nabla^2 = \partial_{xx} + \partial_{yy}$, and ψ is the horizontal streamfunction. Charney was careful, however, to point out that this theory applies only to flows far removed from boundaries and in which variations in the buoyancy frequency N are relatively small. At rigid upper and lower boundaries, the no-normal-flow condition yields a time-dependent conservation equation for buoyancy; when the PV in the interior is assumed to be constant, this boundary condition completely determines the flow, yielding the Surface Quasigeostrophy (SQG) model first discussed by Blumen.[2]

a)Electronic mail: shafer@cims.nyu.edu

At first considered a rather exotic special case, a number of studies have since shown SQG (or variants thereof) to be a relevant model for real atmospheric and oceanic flows. In an atmospheric context, treating the tropopause as a near-rigid lid, Juckes[3] argued that synoptic-scale tropospheric motions are largely determined by temperature anomalies on the tropopause, the latter being well-described by a modified version of SQG. Muraki and Hakim[4] later showed that a next-order extension of SQG may explain observed asymmetries of waves and vortices on the tropopause. Tulloch and Smith[5] constructed a model that includes both surface and interior dynamics and showed that it may explain the atmospheric energy spectrum results of Nastrom and Gage.[6] In an oceanic context, Lapeyre and Klein[7] and, independently, LaCasce and Mahadevan[8] used combined SQG-QG models to reconstruct the three-dimensional interior structure of mesoscale and submesoscale eddying flow from sea surface measurements. Methods of this type have been further explored, developed, and demonstrated in a number of settings.[8–11]

The SQG approach, however, formally applies to surfaces on which the vertical velocity exactly vanishes, yielding (in the quasigeostrophic approximation) a conservation equation for the buoyancy on this two-dimensional surface. Neither the atmospheric tropopause, nor the base of the oceanic mixed layer (to which the SQG-based models apply) are truly rigid surfaces; rather, they are characterized by rapid jumps in stratification N. In the limit of a true discontinuous jump in N (or the vertical shear of the mean horizontal velocity $\partial_z \overline{u}$), the vertical velocity at the jump will vanish, and SQG dynamics will apply; this was shown explicitly by Juckes[3] and Held *et al.*[12] Specifically, if N is taken to be a step function, with the value N_- for $z < 0$ and N_+ for $z > 0$, and if the PV $q = 0$ everywhere except at $z = 0$, then integration of (1) across the discontinuity in q results in the conservation law

$$\partial_t B + J(\psi, B) = 0, \text{ where } B \equiv \left(\frac{f^2}{N^2}\partial_z \psi\right)^+ - \left(\frac{f^2}{N^2}\partial_z \psi\right)^-.$$

In a periodic or infinite domain, the Fourier-transformed elliptic equations given by setting $q = 0$ at wavenumber modulus κ may be solved separately for positive and negative z. Requiring that $\psi \to 0$ as $z \to \pm\infty$ yields decaying exponential functions with scale depths $\kappa N_+/f$ for $z > 0$ and $\kappa N_-/f$ for $z < 0$. This gives the relationship, in Fourier space, between the conserved quantity and streamfunction,

$$B = -\kappa \left(\frac{f}{N_+} + \frac{f}{N_-}\right) \psi \text{ at } z = 0,$$

where κ is the modulus of the horizontal wavenumber. With the linear proportionality to κ, the relationship between B and ψ is exactly analogous to that between the buoyancy $b = f\partial_z \psi$ and streamfunction ψ in the standard SQG model. This should be contrasted with two-dimensional vorticity dynamics, in which the ratio of the conserved quantity (vorticity) to the streamfunction is proportional to κ^2—the difference in the power of the wavenumber is at the heart of the distinct character of flows in the two models.[13,14] Finally, one may be surprised to notice that B does not vanish when $N_+ = N_-$; it is the assumption of a discontinuity in q, rather than in N (although the former presumably follows from the latter) that results in a linear-in-κ relation between conserved quantity and streamfunction. This is related to a central point of this paper, discussed below and in Sec. III.

Here we consider geostrophic turbulence in the presence of a rapid but continuous change in stratification and ask

- How sharp must a jump in N be to generate SQG-like dynamics?
- What are the spatial limits of the SQG-like behavior?

The essence of the effect can be understood by considering the form of the PV with non-constant $N = N(z)$,

$$q = \nabla^2 \psi + \frac{f^2}{N^2}\partial_{zz}\psi - \frac{2N'}{N^3} f^2 \partial_z \psi. \tag{2}$$

At a vertical level $z = z_J$, where N experiences a sharp jump of width h, the derivative N' will be very large, and the buoyancy term will dominate the PV. In some vicinity of this level and some range of horizontal scales, the PV will be negligible compared to its buoyancy-dominated value at z_J, and will be determined by the first derivative of ψ and thus proportional to $\kappa\psi$. Scaling then implies that the remaining terms in the expression for the PV will become important at wavenumbers $\kappa \gtrsim f/(Nh)$, which may be thought of as an inverse deformation scale for the jump-width. In other words, no matter how sharp the jump is, so long as it is smooth, there will always be horizontal scales with associated vertical scales that are small compared to the jump.

We quantify these effects by considering the model stratification $N(z) = N_0[1 + \alpha \tanh(z/h)]$. The control parameter h sets the width of the jump; the model stratification approaches N_0 as $h \to \infty$ and a stepfunction as $h \to 0$, with values $N_+ = N_0(1 + \alpha)$ for $z > 0$ and $N_- = N_0(1 - \alpha)$ for $z < 0$. The effects of the model stratification on the dynamics are investigated first by considering the Green's function for the PV inversion, for which both approximate analytical and numerical forms are constructed. The Green's function is used to make inferences about the vertical and horizontal structure of the energy spectrum under certain assumptions and these predictions are then tested against numerical simulations of the nonlinear equations of motion in the presence of the model stratification and an initial PV anomaly.

Plougonven and Vanneste[15] also considered the effects of a finite-thickness jump in stratification, using a complementary but distinct approach, and addressing a slightly different set of questions. Specifically, they used a matched-asymptotic expansion about the jump region and included the effects of a mean shear, but restricted their attention to linear waves and vanishing PV outside the jump layer. Still, some results in their paper tie directly to results in the present manuscript, as noted in the body of the text.

This paper is organized as follows. In Sec. II we introduce a general Green's function approach to PV inversion and consider closed and approximated forms for a few specific stratification profiles. Section III applies these Green's functions to a set of initial PV distributions, ranging from two extreme limiting cases (height-independent and delta-function) to a specific form that is consistent with the stratification, with q dominated by the third term in (2). Numerical simulations of freely-evolving turbulence, initialized from the latter PV distribution, in the presence of our model stratification, are presented in Sec. IV. Implications and conclusions are discussed in Sec. V.

II. A GREEN'S FUNCTION APPROACH TO PV INVERSION

To facilitate the analysis, we nondimensionalize the buoyancy frequency $N(z)$ by its average N_0, lengths (horizontal and vertical) by a scale H, and define the ratio

$$\sigma = \frac{N_0}{f}.$$

Unless otherwise noted, all quantities are nondimensional from here forward. Upon Fourier transforming in the horizontal, the PV inversion relation may be written

$$\mathcal{L}\psi_\kappa(z) = q_\kappa(z), \quad \text{where} \quad \mathcal{L} = \sigma^{-2}\frac{d}{dz}\frac{1}{N^2(z)}\frac{d}{dz} - \kappa^2 \tag{3}$$

is a self-adjoint operator, ψ_κ and q_κ are the Fourier amplitudes of ψ and q at horizontal wavenumber $\boldsymbol{\kappa}$, and $\kappa = |\boldsymbol{\kappa}|$. The Green's function associated with the inversion problem (3) is the two-variable function $G(z, \xi)$ that satisfies

$$\mathcal{L}G(z, \xi) = \delta(z - \xi) \tag{4}$$

with δ the Dirac function. In an infinite domain, we demand that as $z \to \pm\infty$, the streamfunction $\psi_\kappa \to 0$ and thus $G(z, \xi) \to 0$. It is straightforward to consider finite boundaries, as is done in Tulloch and Smith,[5] but here we wish to focus on the effects of a jump in the stratification at scales removed from the boundaries (nevertheless, some boundary effects will have to be taken into account

for the numerical simulations). In this case, the solution of the inversion is

$$\psi_\kappa(z) = \int_{-\infty}^{+\infty} q_\kappa(\xi) G(z,\xi) d\xi. \tag{5}$$

The Green's function can be written $G(z,\xi) = A(\xi)\phi_+(z)$ for $z \geq \xi$ and $G(z,\xi) = B(\xi)\phi_-(z)$ for $z \leq \xi$, where ϕ_+ and ϕ_- are homogeneous solutions for the regions above and below $z = \xi$, respectively, that satisfy

$$\mathcal{L}\phi_\pm(z) = 0 \quad \text{with} \quad \phi_\pm(z) \to 0 \quad \text{as} \quad z \to \pm\infty. \tag{6}$$

The prefactors $A(\xi)$ and $B(\xi)$ are determined by demanding continuity of $G(z,\xi)$ at $z = \xi$ and that its derivative $\partial_z G(z,\xi)$ at $z = \xi$ has a finite jump. The general solution is then

$$G(z,\xi) = \frac{\sigma^2 N^2(\xi)}{W(\xi)} \begin{cases} \phi_+(z)\phi_-(\xi), & z \geq \xi \\ \phi_+(\xi)\phi_-(z), & z \leq \xi \end{cases}, \tag{7}$$

where $W(\xi) = \phi'_-(\xi)\phi_+(\xi) - \phi'_+(\xi)\phi_-(\xi)$ is the Wronskian and primes denote derivatives with respect to the independent variable.

For constant $N = 1$, the homogeneous problem (6) is trivial to solve and the Green's function takes the form

$$G_0(z,\xi) = -\frac{\sigma}{2\kappa} e^{-\sigma\kappa|z-\xi|}. \tag{8}$$

For arbitrary $N(z)$, a general closed form for G cannot be found and so we turn to a Wentzel-Kramers-Brillouin (WKB) solution, which will be appropriate when $(\sigma\kappa)^{-1} \ll 1$; dimensionally, this is equivalent to assuming horizontal scales small compared to the deformation radius $N_0 H/f$. Because our problem is posed for an infinite domain, this limit is only meaningful once a height scale H is chosen. In practice H can be thought of as the distance to physical boundaries or changes in environment, thus the condition is simply that we consider vertical scales small compared to the vertical extent of the fluid. The WKB solution is described in the Appendix and the resulting approximate Green's function is

$$G(z,\xi) \approx -\frac{\sigma}{2\kappa}\sqrt{N(z)N(\xi)} e^{-\sigma\kappa\left|\int_\xi^z N(u)du\right|}. \tag{9}$$

Note that taking $N = 1$ above recovers the constant-N form G_0 given in (8).

Substitution of the model stratification profile

$$N(z) = 1 + \alpha \tanh(z/h) \tag{10}$$

into (9) gives the WKB-approximated Green's function

$$G_m(z,\xi) \approx -\frac{\sigma}{2\kappa}\sqrt{N(z)N(\xi)} e^{-\sigma h\kappa|\theta(z/h)-\theta(\xi/h)|}, \quad \theta(z) = z + \alpha \ln\cosh z. \tag{11}$$

When $h \to \infty$, the function $h\theta(z/h) \to z$, and G_m reduces to G_0 in (8), the form for $N = 1$. In the opposite limit, when $h \to 0$, the stratification N becomes a step-function, equal to $1 + \alpha$ for $z > 0$ and $1 - \alpha$ for $z < 0$. Considering the positive and negative planes separately, we find G again reverts to its constant-N form G_0, but with σ replaced by $\sigma(1 + \alpha)$ for $z > 0$ and $\sigma(1 - \alpha)$ for $z < 0$; e.g., the only changes are the scaling of the horizontal wavenumber and the associated decay scale from $z = 0$.

III. THE EFFECT OF INITIAL PV DISTRIBUTIONS ON INVERSION

Given the Green's function, determined entirely by the stratification $N(z)$, the q-ψ relationship depends, of course, on the initial PV; consider first the two extreme cases of constant and delta-function PV distributions.

Constant PV distribution: First, consider the extreme example of an initial PV distribution that is independent of z, given by $q_\kappa = Q_\kappa$, a constant that depends only on κ. Along with the

constant-N Green's function (8), the inversion (5) gives

$$\psi_\kappa(z) = Q_\kappa \int_{-\infty}^{\infty} G_0(z,\xi)d\xi = -\frac{Q_\kappa}{\kappa^2}. \tag{12}$$

Here the streamfunction results from an integration of G over all space, resulting in the PV-streamfunction relationship expected for barotropic flows.

We may also consider the case of the z-independent PV distribution with our model stratification (10), though the result is essentially the same. The streamfunction is determined by the integral $\int_{-\infty}^{\infty} G_m(z,\xi)d\xi$, with G_m from (11). This integral doesn't seem to have a closed form, but because $N^{1/2}(\xi)$ is $O(1)$ for all ξ, and $\ln\cosh(\xi/h) \approx |\xi/h| - \ln 2$, the integral turns out to be proportional to $1/\kappa$, and so the streamfunction goes like $1/\kappa^2$, just as before. Thus a height-independent PV distribution will result in a barotropic-like PV-streamfunction relationship, independent of the stratification.

Delta-function PV distribution: Next consider the case where q_κ is sharply peaked at $z = 0$, e.g., take $q_\kappa(z) = \Delta_\kappa \delta(z)$, with Δ_κ a constant depending only on the wavenumber, so that (5) with (8) gives

$$\psi_\kappa(z) = \Delta_\kappa \int_{-\infty}^{\infty} \delta(\xi) G(z,\xi)d\xi = -\frac{\Delta_\kappa \sigma}{2\kappa} e^{-\sigma\kappa|z|}. \tag{13}$$

In this case, the streamfunction picks out the value of the Green's function at the position of the peak in q_κ and thus is proportional to the inverse wavenumber, κ^{-1}, rather than its square.

With the model stratification (10) and a delta-function PV distribution, the result is again the same—the delta-function picks out $G_m(z, 0)$ and no factors of κ are brought down, so the streamfunction goes like $1/\kappa$, as with constant stratification.

The differences in these two extreme cases of peaked- versus constant-PV illustrate that regardless of the form of the stratification, it is the structure of the initial PV distribution that fundamentally changes the character of the relationship between the PV and the streamfunction. In the case of a sharply-peaked initial PV signal, the streamfunction is dominated by the Green's function at the position of the spike in q_κ and its response over all space is slaved to the relationship at this position — this is just what happens in the SQG model. By contrast, when q_κ is independent of z, the streamfunction results from an integration of G over all space, resulting in the relationship between the two fields expected for barotropic flows.

A. PV distribution consistent with model stratification

In the examples above we have taken the PV distribution to be independent of the stratification, but as pointed out in the Introduction, sharp jumps in $N(z)$ will directly affect the PV itself, leading to a dominance of the $\partial_z\psi$ term in the PV-streamfunction relationship. Accordingly we consider a sharply-peaked initial PV distribution with vertical structure given by the third term in (2),

$$q_\kappa(z) = -\frac{\Delta_\kappa}{\sigma^2}\frac{2N'(z)}{N^3(z)}, \tag{14}$$

where $N'(z) = (\alpha/h)\mathrm{sech}^2(z/h)$ is the derivative of the nondimensional buoyancy and Δ_κ is an initial height-independent spectral distribution.[16] The streamfunction, found by integrating the PV distribution against the Green's function in (11), is

$$\psi_\kappa(z) = -\frac{\Delta_\kappa}{2\sigma\kappa} I_\kappa(z/h), \tag{15}$$

where

$$I_\kappa(z) = e^{-\ell\kappa\theta(z)} \int_{-\infty}^{z} F(x) e^{\ell\kappa\theta(x)} dx + e^{\ell\kappa\theta(z)} \int_{z}^{\infty} F(x) e^{-\ell\kappa\theta(x)} dx \tag{16}$$

(which arises after the substitution $x = \xi/h$ has been made), $\ell = \sigma h$ is a deformation scale for the jump,

$$F(x) = \frac{-2\alpha \operatorname{sech}^2 x}{(1 + \alpha \tanh x)^{5/2}} \quad \text{and} \quad \theta(x) = x + \alpha \ln \cosh x.$$

While there is no closed form for the integral, it is useful to analyze its behavior in the limits of small and large wavenumbers.

Small-κ limit: When $\ell\kappa \ll 1$, the sharp peak in $F(x)$ near $x = 0$ means that the integrands are significant only in a small neighborhood around the origin, thus all the exponential factors are approximately 1. When $|z| \gtrsim O(h)$, only the integral that includes 0 inside its limits of integration will contribute to $I(z/h)$ and, in this case, the integral that includes $z = 0$ is approximately $\int_{-\infty}^{\infty} F(x)dx = (4/3)\left[(1+\alpha)^{-3/2} - (1-\alpha)^{-3/2}\right]$. The integration is performed by writing $F(x) = -2N'(x)N^{-5/2}(x) = (4/3)[N^{-3/2}(x)]'$ and noting that $N(x) \to 1 \pm \alpha$ as $x \to \pm\infty$. Finally, noting that $\theta(z) \approx z + \alpha|z|$, the approximate streamfunction in the small-wavenumber limit is

$$\psi_\kappa(z) \approx \frac{2\Delta_\kappa}{3\sigma\kappa}\left[(1+\alpha)^{-3/2} - (1-\alpha)^{-3/2}\right] \begin{cases} 1, & |z| \ll h, \\ e^{-\sigma\kappa(1\pm\alpha)|z|}, & |z| \gtrsim h, \end{cases} \quad \text{for} \quad \ell\kappa \ll 1, \tag{17}$$

where the plus in the exponential applies when $z > 0$ and the negative when $z < 0$. Thus for horizontal disturbance scales large compared to the jump deformation scale $\ell = \sigma h$ (and hence vertical disturbance scales large compared to the jump width h), the PV-streamfunction relationship is similar to that for the delta-function PV distribution (13), with SQG-like behavior near $z = 0$, and exponential decay with e-folding scales $\sim[\sigma\kappa(1 \pm \alpha)]^{-1}$ above (positive) and below (negative) the jump. The important difference here is that the exponential decay starts only for $|z| \gtrsim h$, with the streamfunction (and hence the kinetic energy) nearly constant in a neighborhood about $z = 0$; *the region of active surface dynamics is thus spread out over the thickness of the jump*.

Large-κ limit: In the opposite limit, when $\ell\kappa \gg 1$, we take advantage of the fact that the integrals in (16) are of the Laplace type. Integration by parts gives

$$\int_a^b F(x)e^{\pm\ell\kappa\theta(x)}dx = \pm\frac{F(x)}{\ell\kappa\theta'(x)}e^{\pm\ell\kappa\theta(x)}\Big|_a^b \mp \frac{1}{\ell\kappa}\int_a^b e^{\pm\ell\kappa\theta(x)}\frac{d}{dx}\frac{F(x)}{\theta'(x)}dx$$

and, because $\theta'(x) \neq 0$ and $F(x) \neq 0$ for finite x, the integral on the right is asymptotically smaller than the boundary terms as $\ell\kappa \to \infty$.[17] The boundary terms evaluated at z/h for the two integrals in (16) will add, while the boundary terms at $\pm\infty$ vanish, so that $I_\kappa(z/h) \approx -2F(z/h)/[\ell\kappa\theta'(z/h)]$. In the large-wavenumber limit, then, the streamfunction at $z = 0$ is approximately

$$\psi_\kappa(0) \approx \frac{2\alpha\Delta_\kappa}{(\sigma\kappa)^2 h}, \quad \text{for} \quad \ell\kappa \gg 1. \tag{18}$$

At z away from 0, the expression that arises using the approximation above is less accurate; we neglect the details here, but a full numerical solution to the integral is shown below. The main point is that, at horizontal scales small compared to the jump deformation scale (or vertical scales small compared to h), the wavenumber-dependence of the PV-streamfunction relationship reverts to that for barotropic flow.

At $z = 0$, approximation (17) gives $\psi_\kappa(0) \approx 2\alpha\Delta_\kappa/(\sigma\kappa)$ and (18) gives $\psi_\kappa(0) \approx 2\alpha\Delta_\kappa/(\sigma^2\kappa^2 h)$, implying a transition wavenumber

$$\kappa_t = (\sigma h)^{-1}. \tag{19}$$

Thus, given a finite, smooth jump in background stratification, this is the wavenumber below which the wavenumber dependence of the streamfunction-PV relationship is expected to revert back to its standard $1/\kappa^2$ form, providing a small-scale limit on the applicability of SQG-theory in realistic

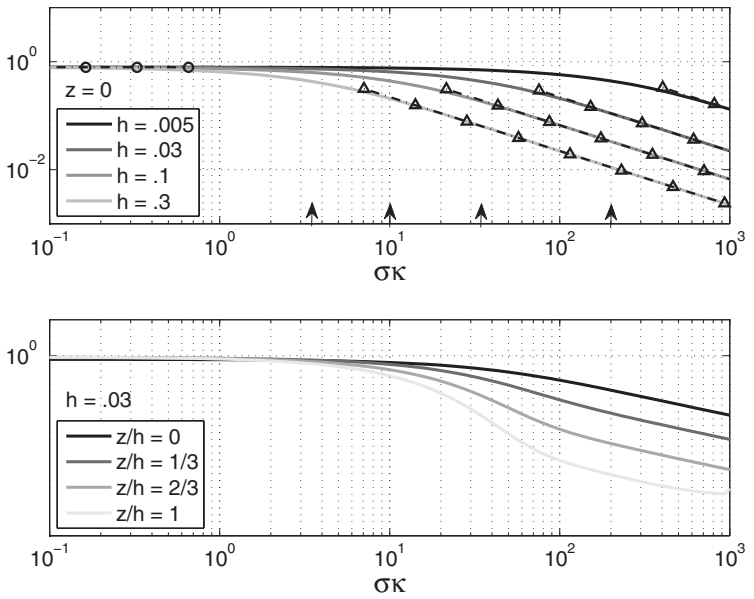

FIG. 1. The spectrum $\sigma\kappa I_\kappa(z/h)$, with $\alpha = 1/3$, plotted against $\sigma\kappa$ on log-log axes. Upper panel: $z = 0$ and h set to the values in the legend. The approximations of I_κ that lead to (17) and (18) are shown as dashed lines with circles and triangles, respectively, and arrows denote the transition wavenumber, κ_t, from (19). Lower panel: the spectrum for $h = 0.03$, at vertical levels listed in the caption.

flows. This small-scale limit of applicability is equivalent to the asymptotic limitation of small perturbation parameter discussed in Plougonven and Vanneste.[15]

Finally, we compute the expected streamfunction for all wavenumbers by numerically integrating (16). The upper panel of Fig. 1 shows $\sigma\kappa I_\kappa(z/h)$, with $\alpha = 1/3$, plotted against $\sigma\kappa$ on log-log axes, for a range of h; multiplication by $\sigma\kappa$ compensates the $(\sigma\kappa)^{-1}$ dependence at small wavenumber. The approximations of $I_\kappa(z/h)$ that lead to (17) and (18) are shown as dashed lines with circles and triangles, respectively. The lower panel shows the same spectrum, for the case $h = 0.03$, for a range of vertical levels extending above the jump. At small wavenumbers, as expected, the spectrum barely changes; however, at large wavenumbers, the spectrum drops off over a broad transition range, returning to a κ^{-1} slope at a reduced magnitude. The main effect of moving away from the jump is an effective decrease in the transition wavenumber. More importantly, at wavenumbers a decade below the transition number, the SQG-like spectrum remains unchanged for vertical levels of $O(h)$ and beyond, above, and below the jump location.

IV. NONLINEAR NUMERICAL SIMULATIONS

Using a dealiased spectral quasigeostrophic model with 512^2 equivalent horizontal points and 400 vertical levels, three numerical simulations of freely-evolving turbulence were conducted on a domain $0 \le x, y < 2\pi$, $-1 \le z \le 1$, in the presence of background stratification given by (10) and initial PV distributions given by (14), with $\sigma = 1$. The three simulations differed only in the value of the jump thickness; the values used were $h = 0.01$, $h = 0.03$, and $h = 0.1$. The wavenumber-dependent constant Δ_κ is set so that the initial energy is 1, distributed isotropically in a gaussian shell about wavenumber $\kappa = 5$, with half-width width 2. The stratification and mean square initial PV and streamfunction are plotted in Fig. 2.

Figure 3 shows snapshots of the PV a few eddy-turnover times after the initial instability, at $z = 0$, for each of the three cases. Close inspection shows a decrease in small-scale structure as h increases, while the flow remains "SQG-like" in all cases; specifically, even for a relatively gentle jump in N, with $h = 0.1$, buoyancy filaments remain unstable to secondary roll-up.

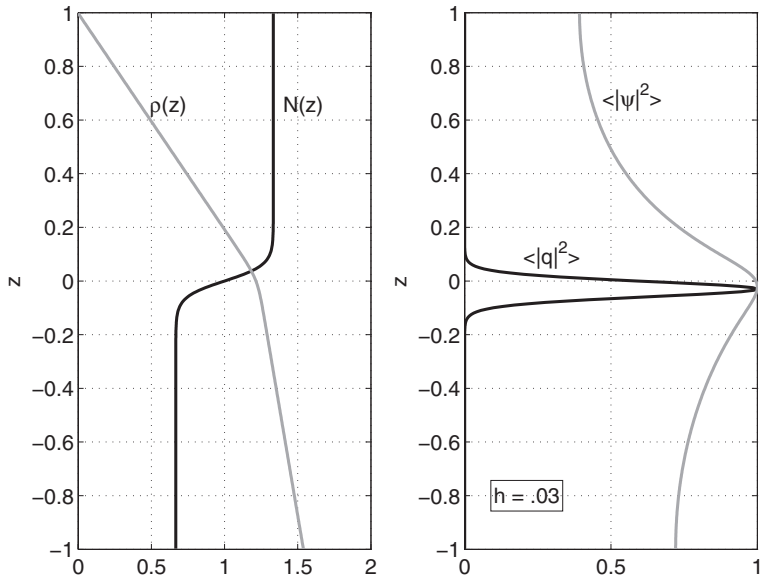

FIG. 2. (Left) Stratification $N(z)$ (black) and density $\rho(z)$ (gray) with $h = 0.03$. (Right) Initial mean square PV profile (black) and streamfunction profile (gray) for case with $h = 0.03$.

For each case, one may also consider how the flow varies as one moves away from the jump position $z = 0$. Figure 4 shows snapshots of the PV at the same point in time, for the case with $h = 0.03$ and $z = 0$, h, $2h$, $4h$, $8h$, $16h$. As expected, the flow becomes less locally-controlled and takes on the appearance of a tracer in the Batchelor regime. This effect is similar to that described by both Scott[18] and Sukhatme and Smith.[19]

Figure 5 shows the horizontal kinetic energy spectra at various vertical levels, for the simulation performed with $h = 0.03$ (see caption for details). The light gray dashed lines represent the predicted spectrum, as follows. Given the streamfunction (15), the azimuthally-averaged horizontal kinetic energy spectrum is

$$\mathcal{K}(\kappa, z) = \left(\frac{L}{2\pi}\right)^2 \int_0^{2\pi} |\psi_\kappa|^2 \kappa^3 d\theta = \frac{I_\kappa^2(z/h)}{4\sigma^2} \mathcal{B}(\kappa), \tag{20}$$

where

$$\mathcal{B}(\kappa) = \left(\frac{L}{2\pi}\right)^2 \int_0^{2\pi} |\Delta_\kappa|^2 \kappa d\theta$$

is the azimuthally-averaged spectrum of $|\Delta_\kappa|^2$. Recall that the form of the initial PV distribution in (14) is based on the third term in (2) and so $\Delta_\kappa \approx \partial_z \psi_\kappa$, the buoyancy, thus $\mathcal{B}(\kappa)$ is effectively

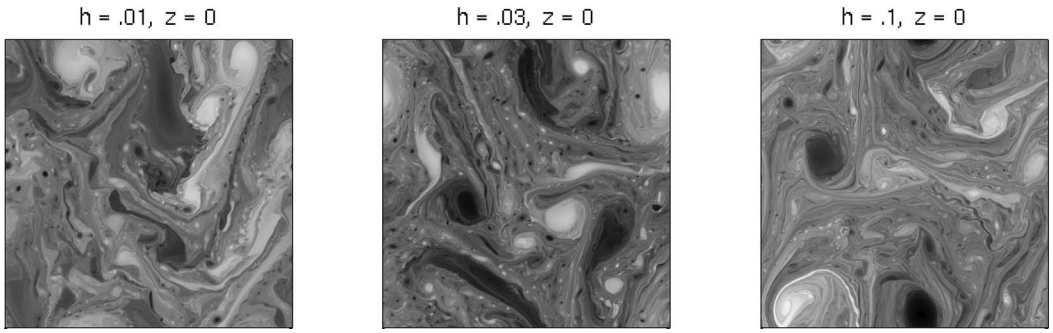

FIG. 3. Horizontal PV slices at $z = 0$ for each of the three simulations.

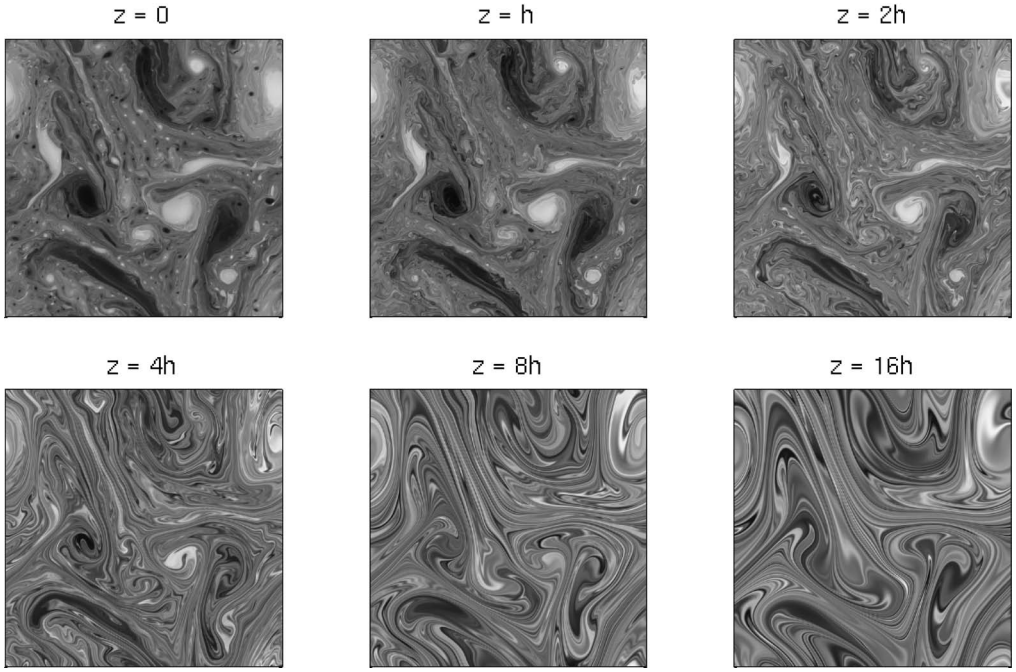

FIG. 4. Horizontal PV slices for the case with $h = 0.03$, at vertical levels from $z = 0$ to $z = 16h$.

the azimuthally-averaged spectrum of the buoyancy variance. At the initial wavenumber, the PV-streamfunction relation is SQG-like ($|q_\kappa| \sim \kappa|\psi_\kappa|$) and so the ensuing forward cascade of buoyancy variance will yield[13] $\mathcal{B}(\kappa) \sim \kappa^{-5/3}$. The theoretical lines in Fig. 5 are thus given by (20), with $\mathcal{B}(\kappa)$ assumed proportional to $\kappa^{-5/3}$, and the entire spectrum normalized to match the energy of the simulated spectrum. The closeness of the fit is remarkable, capturing both the details of the transition to a steeper spectrum at high wavenumbers and the asymmetry above and below $z = 0$.

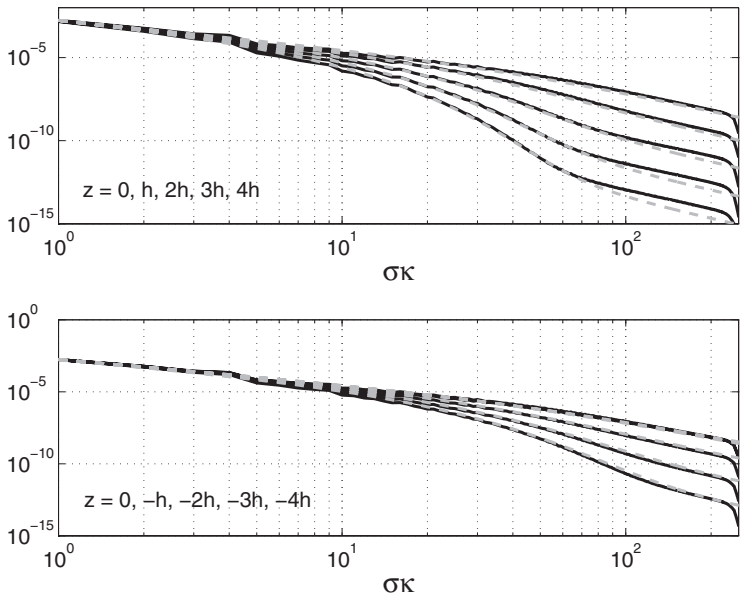

FIG. 5. Kinetic energy spectra at various vertical levels for the simulation with $h = 0.03$ (solid black curves), and the theoretical spectra given by (20) (light gray dashed curves), normalized by the value of the simulated spectra at $\kappa = 1$, and with $\mathcal{B}(\kappa) \sim \kappa^{-5/3}$. (Upper panel) $z = 0$, h, $2h$, $3h$, $4h$. (Lower panel) $z = 0$, $-h$, $-2h$, $-3h$, $-4h$ (the $z = 0$ and $z = -h$ curves are on top of each other).

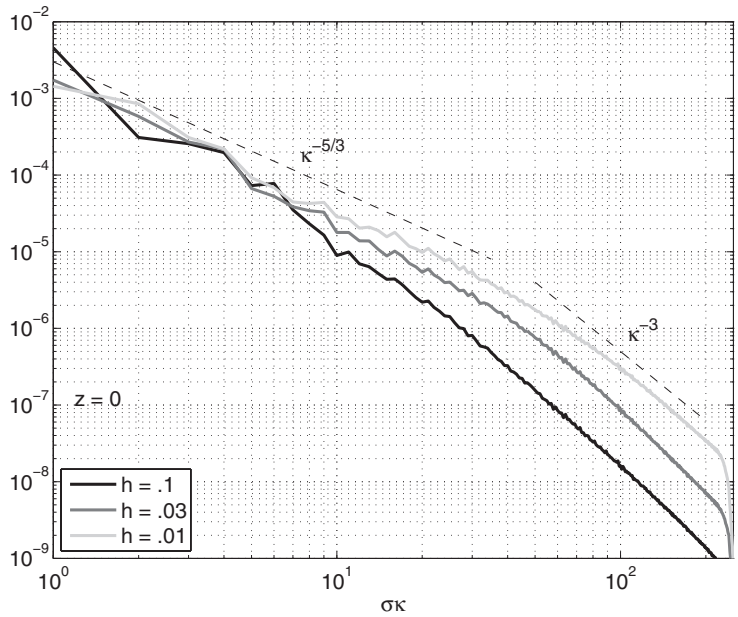

FIG. 6. Horizontal kinetic energy spectra at $z = 0$ for each of the three simulations. The dashed lines are for visual reference, with slopes indicated in the figure.

Finally, Fig. 6 shows horizontal kinetic energy spectra for each of the three cases, at $z = 0$. One can see that, as predicted, and consistent with the visual impression in Fig. 3, the transition to a steeper slope occurs at an increasingly large wavenumber as h decreases.

V. DISCUSSION AND CONCLUSIONS

In quasigeostrophic dynamics, appropriate to small-Rossby-number motions near the deformation scale, the stratification is constant on the timescale of eddies and acts to constrain their nature. Sharp changes in the buoyancy frequency suppresses vertical motions; a discontinuous jump at, say, $z = 0$ yields

$$w|_{z=0} = -\frac{1}{N^2}\frac{Db}{Dt}\bigg|_{z=0} = 0,$$

so that the eddy buoyancy, $b = f\partial_z\psi$, is laterally conserved at the height of the jump. Coupled with the presence of constant PV above and below the jump, the SQG model arises. Neither true discontinuities nor exactly constant PV are found in real geophysical fluids, yet, as described in the Introduction, evidence indicates that behaviors consistent with the SQG model arise in the upper ocean and near the tropopause. Here we have explored an idealization of these regions, with a rapid but continuous change in $N(z)$ and non-constant PV. The goal of the study is to delineate whether, why, where, and on what scales SQG dynamics emerge in such an environment.

The main results follow from the fact that a sharp jump in $N(z)$ yields a peak in the PV and this peak dominates the PV-streamfunction inversion. Considering an initial PV distribution consistent with a jump over a vertical scale h in $N(z)$, we find the following: (1) SQG behavior occurs on lateral scales larger than Nh/f (a deformation scale associated with that jump); (2) at these lateral scales, SQG dynamics is spread vertically over a region proportional the thickness of the jump, and the exponential decay associated with SQG behavior begins only at $|z| \gtrsim h$; (3) at lateral scales smaller than the jump deformation scale, the PV-streamfunction relation reverts to that for barotropic flow.

The stratification profile (10) is too idealized to be applied literally to the atmosphere or ocean. For example, at both the atmospheric tropopause[20] and the base of the oceanic mixed layer,[21] profiles

of $N(z)$ exhibit not just a smooth transition between higher and lower values, but a peak near the more stratified region. Plougonven and Vanneste[15] consider the effects of more realistic profiles of N on edge waves near the tropopause, finding ultimately that the effects of the smooth transition and the enhanced stratospheric stratification cancel one another, strengthening the accuracy of the SQG prediction for edge wave frequencies. We make no attempt to improve the applicability of our model stratification, but the somewhat generic nature of our goals and results seem unlikely to be sensitive to such details.

We consider first implications for the upper ocean. Johnston and Rudnick[21] present observations of the transition region between the mixed layer and the stratified interior, from a large database of high resolution vertical profiles of temperature and salinity. Typical scales from a mid-latitude Pacific track yield estimates $N_0 = 4 \times 10^{-3}$ s^{-1}, $\alpha = 1/2$, and $h^{\#} \simeq 10$ m (the hash distinguishes this dimensional value from the non-dimensional $h = h^{\#}/H$ used throughout the paper), thus $N_0 h^{\#}/f \simeq 200$ m, so that SQG-like behavior is to be expected over the whole submesoscale range of O (1 km) to O (100 km). Notably, the transition layer thickness is much less than the depth of the mixed layer itself, about 100 m in these observations. Note also that, while the assumption $z \to \pm\infty$ is not particularly appropriate for the upper ocean, this could be ameliorated by including a rigid upper boundary in the Green's function inversion. Likewise, one could consider more complex models for $N(z)$ to provide a more realistic model for the oceanic stratification.

As discussed in the Introduction, another application of the present study is to establish limits on the relevance of SQG theory to turbulent dynamics on the tropopause. If, as suggested by Tulloch and Smith,[5] the $-5/3$ mesoscale energy spectra observed in Nastrom and Gage[6] at the tropopause results from a forward cascade of temperature variance, then the finite thickness of the tropopause may limit the range of horizontal and vertical scales over which the mesoscale spectrum holds. Concern about the vertical extent of the predicted spectrum in the model of Tulloch and Smith,[5] and thus its relevance to the atmosphere, led to a comment on that paper by Lindborg,[22] and a subsequent reply by Smith and Tulloch.[23] We revisit those concerns in the context of the present results.

Observations by Birner[20] indicate a near discontinuous jump in stratification at the tropopause: from high-resolution radiosonde observations of the atmospheric stratification, averaged annually relative to the tropopause height, Birner finds an extremely sharp transition from tropospheric to stratospheric N^2 values, occurring over distances of order the effective vertical resolution, about 150 m. In mid-latitudes N^2 jumps from about 2×10^{-4} s^{-2} in the troposphere to nearly 6.5×10^{-4} s^{-2} at the base of the stratosphere, then relaxing, over about a kilometer to 4.5×10^{-4} s^{-2}. One might thus conservatively estimate the parameters for our idealized profile with $N_0 = 1.8 \times 10^{-2}$ s^{-1}, $\alpha = 1/4$, and $h^{\#} \sim 300$ m, so as an upper limit, the "jump deformation scale" $L_J = N_0 h^{\#}/f$ is about 75 km, which is close to the end of the $-5/3$ mesoscale energy spectra of Nastrom and Gage.[6] The ratio L_J/L_D, where L_D is the midlatitude atmospheric internal deformation, is equivalent to the nondimensional tropopause thickness $h = h^{\#}/H = L_J/L_D$. Taking $L_D \simeq 2500$ km, the non-dimensional thickness $h \simeq 0.03$, just as for the simulation presented in Fig. 5. Dimensionally, L_D is the scale associated with $\kappa = 1$ in the figure and, so, even at a distance of $4h$ below the "tropopause" $z = 0$, the spectrum retains a $-5/3$ slope down to horizontal scales a decade smaller than L_D. Thus, the present model would imply a flattened mesoscale spectrum extending at least half a kilometer below the tropopause. However, there are far too many simplifications made in the idealized model presented here to take this estimate seriously; we wish to point out only that, over a wide range of scales below L_D, the vertical extent of the flattened mesoscale spectrum should be far larger than one would assume from the basic SQG model.

ACKNOWLEDGMENTS

This work was begun while E. Bernard was a visiting student at the Courant Institute in 2010. The authors thank Shane Keating, Jacques Vanneste, and Xiao Xiao for helpful comments. K.S.S. is supported by NSF (Grant No. OCE-0962054) and ONR (Grant No. N00014-09-01-0633).

APPENDIX: WKB SOLUTION FOR THE GREEN'S FUNCTION

Expanding the derivative and multiplying by $N^2(z)/\kappa^2$, the homogeneous problem (6) can be written as

$$\varepsilon^2\phi_\pm'' - \varepsilon^2\frac{2N'(z)}{N(z)}\phi_\pm' - N^2(z)\phi_\pm = 0,$$

where $\varepsilon \equiv (\sigma\kappa)^{-1}$ and primes denote derivatives with respect to z. A WKB solution will be appropriate when $\varepsilon \ll 1$, which is equivalent to assuming horizontal scales small compared to N_0H/f (recall that H is set to 1), as discussed in Sec. II. A WKB approximation is found by expanding the solutions $\phi_\pm(z)$ as

$$\phi_\pm(z) \sim \exp\left[\frac{1}{\gamma}\sum_{n=0}^{\infty}\gamma^n S_n^\pm(z)\right],$$

where γ is a small parameter. Truncation of the expansion at $n = 1$ (the "physical optics" approximation), substitution into (6), and demanding dominant balance gives $\gamma = \epsilon$, from which it follows that $S_0^\pm(z) = \mp\int^z N(u)du$ and $S_1(z) = (1/2)\ln N(z)$. Application of the appropriate boundary conditions in (6) then gives

$$\phi_\pm(z) \sim \sqrt{N(z)}\exp\left[\mp\sigma\kappa\int^z N(u)du\right]$$

and substitution into (7) gives the approximate Green's function given in (9).

[1] J. G. Charney, "Geostrophic turbulence," J. Atmos. Sci. **28**, 1087–1095 (1971).
[2] W. Blumen, "Uniform potential vorticity flow: Part I. Theory of wave interactions and two-dimensional turbulence," J. Atmos. Sci. **35**, 774–783 (1978).
[3] M. N. Juckes, "Quasigeostrophic dynamics of the tropopause," J. Atmos. Sci. **51**, 2756–2768 (1994).
[4] D. J. Muraki and G. J. Hakim, "Balanced asymmetries of waves on the tropopause," J. Atmos. Sci. **58**, 237–252 (2001).
[5] R. Tulloch and K. S. Smith, "Quasigeostrophic turbulence with explicit surface dynamics: Application to the atmospheric energy spectrum," J. Atmos. Sci. **66**, 450–467 (2009).
[6] G. D. Nastrom and K. S. Gage, "A climatology of atmospheric wavenumber spectra of wind and temperature observed by commercial aircraft," J. Atmos. Sci. **42**, 950–960 (1985).
[7] G. Lapeyre and P. Klein, "Dynamics of the upper oceanic layers in terms of surface quasigeostrophy theory," J. Phys. Oceanogr. **36**, 165–176 (2006).
[8] J. H. LaCasce and A. Mahadevan, "Estimating subsurface horizontal and vertical velocities from sea surface temperature," J. Mar. Res. **64**, 695–721 (2006).
[9] P. Klein, B. L. Hua, G. Lapeyre, X. Capet, S. L. Gentil, and H. Sasaki, "Upper ocean turbulence from high resolution 3D simulations," J. Phys. Oceanogr. **38**, 1748–1763 (2008).
[10] J. Isern-Fontanet, G. Lapeyre, P. Klein, B. Chapron, and M. W. Hecht, "Three-dimensional reconstruction of oceanic mesoscale currents from surface information," J. Geophys. Res. [Oceans] **113**, C09005, doi:10.1029/2007JC004692 (2008).
[11] P. Y. Le Traon, P. Klein, and B. L. Hua, "Do altimeter wavenumber spectra agree with the interior or surface quasigeostrophic theory?" J. Phys. Oceanogr. **38**, 1137–1142 (2008).
[12] I. M. Held, R. T. Pierrehumbert, S. T. Garner, and K. L. Swanson, "Surface quasi-geostrophic dynamics," J. Fluid Mech. **282**, 1–20 (1995).
[13] R. T. Pierrehumbert, I. M. Held, and K. L. Swanson, "Spectra of local and nonlocal two-dimensional turbulence," Chaos, Solitons Fractals **4**, 1111–1116 (1994).
[14] K. S. Smith, G. Boccaletti, C. C. Henning, I. N. Marinov, C. Y. Tam, I. M. Held, and G. K. Vallis, "Turbulent diffusion in the geostrophic inverse cascade," J. Fluid Mech. **469**, 13–48 (2002).
[15] R. Plougonven and J. Vanneste, "Quasigeostrophic dynamics of a finite-thickness tropopause," J. Atmos. Sci. **67**, 3149–3163 (2010).
[16] Note that if we take $q_\kappa(z)$ to be literally the third term in (2), then $\Delta_\kappa = \partial_z\psi_\kappa$, implying that the streamfunction is linear in z. Instead, we demand that (14) be true and find the streamfunction using the Green's function.
[17] C. M. Bender and S. A. Orszag, *Advanced Mathematical Methods for Scientists and Engineers* (Springer-Verlag, New York, 1999), p. 258.
[18] R. K. Scott, "Local and nonlocal advection of a passive scalar," Phys. Fluids **18**, 116601 (2006).
[19] J. Sukhatme and L. M. Smith, "Local and nonlocal dispersive turbulence," Phys. Fluids **21**, 056603 (2009).
[20] T. Birner, "Fine-scale structure of the extratropical tropopause region," J. Geophys. Res. **111**, D04104, doi:10.1029/2005JD006301 (2006).
[21] T. M. S. Johnston and D. L. Rudnick, "Observations of the transition layer," J. Phys. Oceanogr. **39**, 780–797 (2009).
[22] E. Lindborg, "Two comments on the surface quasigeostrophic model for the atmospheric energy spectrum," J. Atmos. Sci. **66**, 1069–1072 (2009).
[23] K. S. Smith and R. Tulloch, "Reply," J. Atmos. Sci. **66**, 1073–1076 (2009).